Geochemistry Exploration and Geothermometry Application in the North Zone of Seulawah Agam, Aceh Besar District, Indonesia

Rinaldi Idroes [1,*] **, Muhammad Yusuf** [1]**, Saiful Saiful** [1]**, Muksin Alatas** [1]**, Subhan Subhan** [1]**, Andi Lala** [1]**, Muslem Muslem** [1]**, Rivansyah Suhendra** [2]**, Ghazi Mauer Idroes** [3]**, Marwan Marwan** [4] **and Teuku Meurah Indra Mahlia** [5]

[1] Department of Chemistry, Faculty of Mathematics and Natural Sciences, Universitas Syiah Kuala, Banda Aceh 23111, Indonesia; iamyusufibrahim@gmail.com (M.Y.); saiful@unsyiah.ac.id (S.S.); mukhsinmuhaddis@gmail.com (M.A.); subhanaan18@gmail.com (S.S.); andy_beck42@yahoo.com (A.L.); moslem_coolam@yahoo.com (M.M.)

[2] Department of Informatics, Faculty of Mathematics and Natural Sciences, Universitas Syiah Kuala, Banda Aceh 23111, Indonesia; rivans.suhendra@gmail.com

[3] Department of Chemical Engineering, Faculty of Engineering, Universitas Syiah Kuala, Banda Aceh 23111, Indonesia; Idroesghazi@gmail.com

[4] Department of Geophysic Engineering, Faculty of Engineering, Universitas Syiah Kuala, Banda Aceh 23111, Indonesia; marwan.geo@unsyiah.ac.id

[5] School of Information, Systems and Modelling, University of Technology Sydney, Sydney, New South Wales 2007, Australia; tmindra.mahlia@uts.edu.au

* Correspondence: rinaldi.idroes@unsyiah.ac.id; Tel.: +62-819-7374-4077

check for updates

Abstract: A geochemistry study has been done in four geothermal manifestations—*Ie-Seu'um*, *Ie-Brôuk*, *Ie-Jue* and the Van-Heutz crater—located in the north zone of Seulawah Agam mountain (Aceh Besar District, Indonesia). The study was performed through water and gas analysis. Water analysis were done for all geothermal manifestations, but gas analysis was only done for the *Ie-Jue* manifestation that has fumaroles. Cation and anion contents were analyzed by ion chromatography, ICP-OES, alkalimetry titrations, and spectrophotometry, meanwhile isotopes were measured by a Liquid Water Isotope Analyzer. The resulting data were used for fluid and gas geothermometry calculations, and plotted in a FT-CO_2 Cross-Plot and a CH_4-CO_2-H_2S triangle diagram to obtain reservoir temperatures. The data were also plotted by a Cl-HCO_3-SO_4 triangle and Piper diagram to obtain the water type and dominant chemical composition, a Na-K-Mg triangle diagram to obtain fluid equilibria, the isotope ratio in the stable isotope plot to obtain the origin of water, and a N_2-He-Ar triangle diagram to establish the origin of fumaroles. The water analysis results showed that (1) *Ie-Seu'um* has an average reservoir temperature of 241.9 ± 0.3 °C, a chloride water type, a dominant Na-K-Cl chemical composition, a mature water fluid equilibrium, and water of meteoric origin; (2) *Ie-Brôuk* has an average reservoir temperature of 321.95 ± 13.4 °C, a bicarbonate water type, a dominant Na-Ca-HCO_3 chemical composition, an immature water fluid equilibrium, and water of meteoric origin; (3) *Ie-Jue* has an average reservoir temperature of 472.4 ± 91.4 °C, a sulphate water type, a dominant Ca-SO_4 chemical composition, an immature water fluid equilibrium and water of meteoric origin; and (4) the Van-Heutz crater has an average reservoir temperature of 439.3 ± 95.3 °C, a sulphate water type, a dominant Ca-SO_4 chemical composition, an immature water fluid equilibrium and water of magmatic origin. The results of our gas analysis showed that *Ie-Jue* has an average reservoir temperature of 258.85 °C, and water of meteoric origin. Based on the reservoir temperatures, the geothermal manifestation of the north zone of Seulawah Agam mountain is considered as a high-temperature geothermal system suitable for power plant development.

---

1. Introduction

The environmental impact due to global warming has reaching a point from which there is no return. According to researchers the main culprit of global warming are the greenhouse gases, especially carbon dioxide, released by energy consumption for human activities [1]. One of the ways to solve this problem is by using renewable energy sources for energy generation, and many countries have successfully implemented renewable energy policies [2]. Some countries have successfully implemented solar energy as an electricity source to support daily life activities [3,4], however, the problem with solar energy sources is that it is only available for certain periods and therefore energy storage devices must be used. The only storage devices commercially available at this moment are batteries, which have very limited capacity and therefore scientists are attempting to find new energy storage materials [5,6]. Like some other countries Malaysia and Indonesia have successfully implemented biodiesel energy policies to power their transport sector [7–9]. However, this policy has been claimed by some researchers to create conflicts with food production and destroy the tropical rain forest. Therefore, Indonesia is trying to encourage the use of cleaner energy sources such as geothermal energy for electricity generation to replace fossil fuels.

Since 1970, Indonesia has undertaken geothermal explorations in order to discover and develop high-temperature geothermal energy sources [10]. Indonesia contains 13% of the total world's volcanoes, of which 80% are estimated to possess geothermal energy production potential [11]. Those volcanoes are spread over 312 locations [12] with an average estimated geothermal potential of around 28.617 MWe which is equal to 40% of the total world's geothermal potential [13]. Nevertheless, only 4.7% of them have been explored and exploited for electrical energy resources, providing a capacity of 1340 MWe from 10 geothermal wells [12]. They are: Darajat (260 MWe), Dieng (60 MWe), Kamojang (200 MWe), Salak Mountain (377 MWe), Sibayak (12 MWe), PLTP Wayang Windu (227 MWe), Lahendong (87 MWe), Ulu Belu-Sumatera Selatan (110 MWe), Ulumbu-Flores (5 MWe) and Mataloko (2.5 MWe). Apart from the stated above, there are an additional 440 MWe of geothermal energy under construction in Sarulla and Lumut Balai. However, the geothermal energy capacity that is under exploitation is considered small compared to Indonesia's short-medium term development target of geothermal electrical capacity for 2025, which is around 6000 MWe, equal to 5% of the national energy demand [12].

A geothermal system location can be exploited if the exploration results data are previously determined. Geothermal exploration and modeling cover three components, which are geological, geophysical and geochemical studies. The main objective of geochemical research is to estimate the temperature that can be obtained from the geothermal system. A high-temperature geothermal system can provide a high geothermal energy capacity. To obtain such information, it is necessary to carry out fluid-geochemistry analysis, which includes hydro-geochemical, gas-geochemical and isotope analyses. Apart from geothermal temperature, the geochemical study also informs the origin of the geothermal system and geochemical processes that affect the fluid's temperature. Recently, geochemical studies on geothermal systems have been many conducted in various sites around the world, including Kangding in the eastern Himalayas [14]; the Icelandic high-temperature geothermal areas [15]; the western sector of the Sabatini Volcanic District and the Tolfa Mountains (Italy) [16]; the Xining basin on the northeastern Tibetan Plateau [17]; Mapamyum in Western Tibet, China [18]; the Tang-Bijar oilfield springs in the Zagros region of Iran [19]; southern Saint Lucia, in the Lesser Antilles island arc [20]; the Southern Sula graben in Honduras [21]; and the Nevşehir (Kozakli) area in Central Turkey [22].

Almost half of the geothermal potential in Indonesia is found on the island of Sumatra, one which is in Seulawah Agam in Aceh Province. Seulawah Agam's geothermal site has several manifestations,

that are *Ie-Su'um, Ie-Brôuk, Ie-Jue* and the Van-Heutz crater in the north zone, and the *Aleu Ie Su'um*, *Alue Ie Masam*, *Alue PU* and *Alue Teungku* manifestations in the south zone. Some studies have been done in this area. Geophysical studies of geothermal resource imagery [23] and deep and shallow structures of geothermal sites [24] have been done in the Seulawah Agam area. Preliminary geochemical studies have also done at three manifestations of the North Zone, which are the *Ie Su'um* [25], *Ie Ju* [26] and *Ie-Brôuk* [27] ones. Estimated depth temperature, type of geothermal water, chemical composition and fluid equilibrium of the three manifestations is predicted with hydro-geothermometry in calculating cations and anions analyzed by atomic absorption spectrophotometry (AAS) and UV-Vis spectrophotometry.

Geothermal potential determination is a complex process. There are many hydrogeochemical processes that affect the fluid emigrating from the source to the surface. This causes the unrelibleness of reservoir temperature predictions based on only a single geothermometry method. Thus, hydro-geothermometry, gas-geothermometry, and isotopic methods (if available) should be applied together. Besides, the chemical identification needs to be accurate using a sensitive instrument. Especially for atomic analysis, spectra identification in a plasma gives more precise and reliable results [28,29]. The accuracy of the measurement determines the geothermometry calculations, hence determining the estimated temperature of the manifestation reservoir.

Refractory compound formation always deserves attention in elemental analysis. The sample may contain constituents that form a refractory (heat-stable) compound with the analyte element of interest, and is avoided by addition of a chemical competitor or use of very high temperatures such as in inductively coupled plasma (ICP). ICP uses a 3–4× higher temperature, is 100–1000× more sensitive and has a 2–3× higher linear range than flame spectrometry. In nature there are many metal oxides. The low temperatures of flame atomic spectrometry sometimes cause the spectrum to be the result of metal oxide molecules, not the desired atomic line spectrum. This is very disturbing for the accuracy.

In this study, a geochemical exploration has been conducted on some geothermal areas in the north zone of Seulawah Agam mountain, which are the *Ie-Seu'um*, *Ie-Brôuk*, *Ie-Jue*, and the Van Heutz-crater manifestations. The study includes in-situ, liquid geothermal, gas geothermal, and isotope analysis. Ions in the liquid and gas were analyzed with ICP-OES, ion-chromatography, UV-Vis spectrophotometry and alkalimetry titration. Isotope analysis was carried out by laser spectroscopic analysis. Several geothermometry methods were applied to obtain geochemical data, including hydro-geothermometry, gas-geothermometry, and stable isotope plots to provide information on the types, chemical composition and liquid equilibrium, reservoir temperature predictions and the origin of the geothermal fluid.

2. Study Area

This study covers the area in the north zone of Selawah Agam mountain (Figure 1). At this location, there are four geothermal system manifestations, which are *Ie-Seu'um*, *Ie-Brôuk, Ie-Jue*, and the Van-Heutz crater manifestations.

Sampling points were established at each geothermal system manifestation, which were SH1, SH2, and SH3 in *Ie-Seu'um*; IB1 and IB2 in *Ie-Brôuk*; JH1, JH2, JH3 and JH4 in *Ie-Jue*; and VH1, VH2, and VH3 in the Van-Heutz crater. Based on the physical observation of the condition of the north zone in the *Ie-Seu'um* manifestation, it appears to have clear spring water. It is found that the water discharge at SH2 is bigger than at SH1 and SH3. The surface characteristic is observed to have sediment on the brown color rocks that resembles silica sinter. In the *Ie-Jue* manifestation, the hot spring is found to be muddy and full of gases. Meanwhile in the *Ie-Brôuk* manifestation, a moderate hot spring is found to be around the puddle and have a few air bubbles, where several aquatic species, such as leeches, are found. In the Van-Heutz crater manifestation the water output appears to have high turbidity and acidic pH. The manifestation is located in a crater, thus being a source of solfatara output gas with a light yellow color that is found around the manifestation.
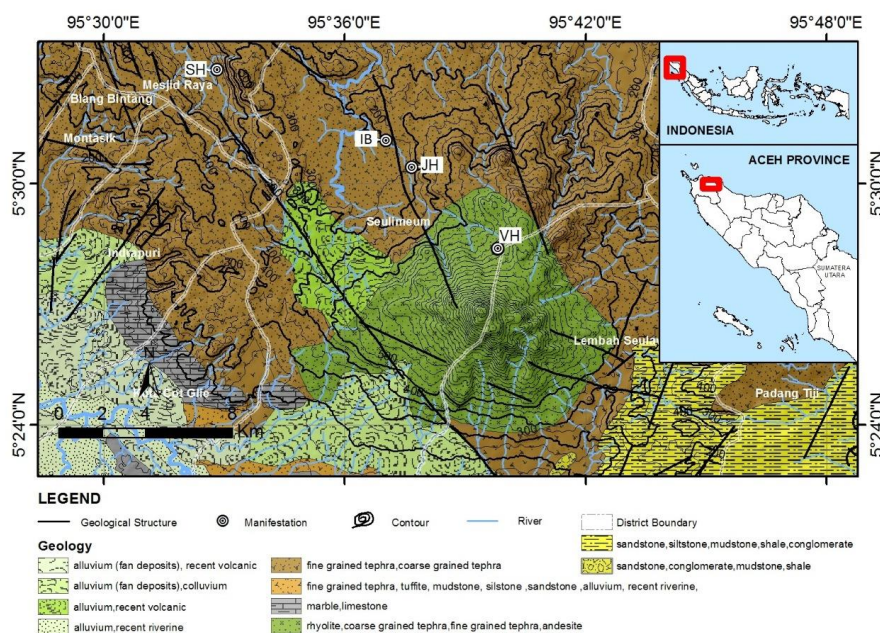
Figure 1. Geological Map of Seulawah Agam Mountain, Aceh Besar district, Indonesia. Sampling point codes; SH (*Ie-Seu'um*); IB (*Ie-Brôuk*); JH (*Ie-Jue*); VH (Van-Heutz crater).

3. Materials and Methods

3.1. Field Observation Equipment

The observation equipment (general equipment) used, which included latex gloves, waterproof markers, compass, notebooks, camera, trekking poles, sulphur detector, boots, and a first-aid kit, follows Nicholson [30].

3.2. Water Sampling and Analysis

Water sample collection was carried out at the four manifestations of the north zone: the *Ie-Seu'um*, *Ie-Jue*, *Ie-Brôuk* and Van-Heutz crater manifestations. The coordinates and elevation data of each sampling point was marked by GPS (62S, Garmin, Olathe, KS, USA). Water samples were collected and put in polyethylene (PE) bottles. The bottles are then placed in a cooling box and transported to the laboratory for cation, anion, SiO_2, and isotope (δD dan $\delta^{18}O$) analysis.

During the placement of the water samples into the bottles, 6 N HNO_3 was added to the samples for cation analysis until the pH reached <2 (acidified). On the other hand, for anion analysis, nothing is added to the samples (non-acidified). Samples for SiO_2 analysis were diluted in deionized water to prevent the precipitation of silica. Before the analysis, water samples were filtered with Whatmann 0.45 μm filter paper.

An in-situ analysis is done at the hot spring sampling locations. The analysis includes the determination of water surface temperature using a thermometer (Fisher Scientific Traceable, Fisher Scientific, Hampton, NH, USA), acidity level using a pH meter (Schott Instruments, Xylem Analytics, Mainz, Germany), conductivity using a conductometer (Schott Instrument) and Total Dissolved Solids (TDS) using a TDS meter (Hanna, Hanna Instruments, Woonsocket, RI, USA). Each determination is repeated five times to obtain average values and uncertainty values (standard deviations).

Cation analysis (K, Na, Mg, Ca, Li, B) was carried out by Inductively Coupled Plasma-Optical Emission Spectrometry (ICP-OES, iCAP 7400 instrument, Thermo Fisher Scientific, Waltham, MA, USA) in a wavelength range from 166 to 847 nm with argon as combustion gas. Anion analysis (SO_4, F, Cl, NO_3) was carried out by ion chromatography (IC Plus 883, Metrohm, Herisau, Switzerland) using a Metrosep A Supp 5–150/4.0 column, eluent composition 1 mmol L^{-1} $NaHCO_3$ + 3.2 mmol L^{-1} Na_2CO_3

dissolved in aquabidest and acetone (980 mL aquabidest and 20 mL acetone), 0.700 mL min^{-1} flow rate and 9.63 MPa pressure. SiO_2 analysis is carried out with a UV-Vis spectrophotometer (Genesys 10S, Thermo Scientific) employing a standard method [31]. HCO_3^- ion analysis is conducted by the alkalimetry titration method. Isotope (δD and $\delta^{18}O$) analysis is carried out by laser spectroscopic analysis (LGR DT−100 Liquid Water Stable Isotope Analyzer, Los Gatos Research, Inc., San Jose, CA, USA). The liquid samples are measured according to the calibration standard and control standard. The obtained isotope ratio is correlated with the Vienna Standard Mean Ocean Water (VSMOW) international standard plot, with analysis precision standard under 0.6‰ for δD and 0.1 ‰ for $\delta^{18}O$ [32].

3.3. Gas Sampling and Analysis

Gas (also known as fumarole gas) samples were collected from fumarole sources at the *Ie-Jue* manifestation location. Gas was collected in Giggenbach flasks using the standard gas sampling technique method as explained by Giggenbach and Goguel [33]. An evacuated Giggenbach bottle containing 100 mL NaOH 4 N and a little $CdCl_2$ indicator was used. First the hose that connects the gas source and Giggenbach bottle was checked for leaks to avoid any contamination by outside air. The valve of the Giggenback bottle was opened to let the gas enter the bottle while shaking to accelerate the gas dissolution process in the $NaOH/CdCl_2$ solution. The process is ended by closing the valve when the vacuum in the Giggenbach bottle is about to run out. The collected gas sample is then transported to the laboratory for analysis. The analysis of the gaseous samples is conducted using two methods: a gas chromatography method for unreactive gases (H_2, Ar, N_2, and CH_4) using a GC-TCD (HP−5890 system company, Agilent Technologies, Santa Clara, CA, USA) equipped with a Porapak column, and a titration method for reactive gases (CO_2, NH_3 and H_2S).

3.4. Geothermometry Applications

3.4.1. Hydro-Geothermometry

The depth temperature is calculated by the Na-K geothermometer equation [34–39] and Na-K-Ca geothermometry [40]. The dissolved chemical equilibrium is determined by a Na-K-Mg triangle diagram [34]. Dominant cation-anion content is estimated by a Piper diagram [41]. The geothermal water type is determined by a Cl-SO_4-HCO_3 triangle diagram [42]. The equations of each geothermometry technique used are presented in Table 1.

Table 1. Temperature equations (°C) for geothermometry.

Geothermometer	Equations	References
Na–K	T = [855.6 / (0.857 + log(Na/K))] − 273.15	[37]
Na–K	T = [833 / (0.780 + log(Na/K))] − 273.15	[36]
Na–K	T = [1319 / (1.699 + log(Na/K))] − 273.15	[39]
Na–K	T = [1217 / (1.483 + log(Na/K))] − 273.15	[35]
Na–K	T = [1178 / (1.470 + log(Na/K))] − 273.15	[38]
Na–K	T = [1390 / (1.750 + log(Na/K))] − 273.15	[34]
Na-K-Ca	$T = \dfrac{1647}{\log \frac{Na}{K} + \beta \left[\log \left(\frac{Ca}{Na} \right) + 2{,}06 \right]} - 273.15$ for: β = 4/3, if T < 100 °C β = 1/3, if T > 100 °C	[40]

3.4.2. Gas Geothermometry

The depth temperature is estimated by the gas geothermometry equations shown in Table 2. The depth temperature is also estimated by a Grid Fischer-Tropsch CO_2 (FT-CO_2) diagram [42] and CH_4-CO_2-H_2S diagram grid [43]. The origin of the gas fluid is estimated by a N_2-He-Ar triangle diagram [34].

Table 2. Temperature equations (°C) for gas geothermometers.

Geothermometer	Formula (°C)	Reference
$CO_2/H_2S/CH_4/H_2$	$T = \dfrac{24775}{\left[2\log\left(\frac{CH4}{CO2}\right)-6\log\left(\frac{H2}{CO2}\right)-3\log\left(\frac{H2S}{CO2}\right)+7\log P_{CO_2}+36.05\right]} - 273.15$	[44]
H_2/Ar	$T = 70[2.5 + \log(m_{H2}/m_{Ar})]$	[33]
CH_4/CO_2	$T = \dfrac{4625}{10.4+\log\left(\frac{CH4}{CO2}\right)} - 273.15$	[42]
CO_2/H_2	$T = 341.7 + 28.57 \ \log m_{CO2/H2}$	[42]

3.5. Uncertainty of Measurement

All data analysis was carried out using Spreadsheet Version 3 of Powell Geoscience Ltd. (3 September 2012) by Powell and Cumming (Microsoft Corporation, Redmond, WA, USA). Uncertainty of the concentration measurements of each parameter is presented in standard deviation values and several statistical function data using the LINEST method in Microsoft Excel (Microsoft Corporation, Redmond, WA, USA) The calculation results obtained the statistical function data including slope (m), standard deviation of slope (S_m), intercept (b), standard deviation of intercept (S_b), determination coefficient (R), standard deviation of regression (S_r) and standard deviation of the concentration (S_C) [45]. The equations used in the calculation of standard deviations and statistic functions are presented in Table 3.

Table 3. Calculation formula of measurement uncertainty.

Name	Formula	Reference
Standard deviation of regression	$Sr = \sqrt{\dfrac{S_{yy}-m^2S_{xx}}{N-2}}$	
Standard deviation of slope	$S_m = \sqrt{\dfrac{S_y^2}{\sum \ (\overline{X}-X_i)^2}} = \sqrt{\dfrac{S_y^2}{\sum \ x_i^2-(\sum \ X_i)^2/N}}$	[45]
Standard deviation of intercept	$S_b = S_y \sqrt{\dfrac{S_y^2 \ \sum \ X_i^2}{N\sum \ X_i^2-(X_i)^2}} = \ S_y \sqrt{\dfrac{1}{N-(\sum \ X_i)^2/\sum \ X_i^2}}$	
Standard deviation of the concentration	$Sc = \dfrac{S_r}{m} \sqrt{\dfrac{1}{M} + \dfrac{1}{N} + \dfrac{(Y_c-Y_{ave})^2}{m^2S_{xx}}}$	

4. Results and Discussion

4.1. Measurement Data

4.1.1. Hydrothermal Characteristics

The results of in-situ measurements such as temperature, pH, conductivity, and total dissolved solids (TDS) as the representative surface characteristic data of the hot spring manifestations in the north zone of Seulawah Agam mountain are listed in Table 4. The obtained data suggest variations for each manifestation point. The manifestation temperature range is from warm (40.04 °C) to hot (98.62 °C). The acidity of the *Ie-Seu'um* and *Ie-Brôuk* manifestations is in the pH 6.66–7.40 range (neutral), the *Ie-Jue* manifestation is at pH 3.95–5.93 (acidic), while the Van Heutz crater manifestation is in the pH range of 1.81–1.44 (highly acidic). The conductivity and TDS of *Ie-Seu'um, Ie-Jue* and *Ie-Brôuk* are high, in the range of 14.02–215.78 mV and 237.60–1766 mg L^{-1}, respectively, while the conductivity and TDS of the Van-Heutz crater manifestation is very low, in the range of 7.28–9.67 mV and 3.64–4.85 mg L^{-1}, respectively.

Table 4. Characteristics of surface manifestation of the north zone, Seulawah Agam mountain.

No	Locations	Sampling Points	Coordinates		Elevation (m)	Twater (°C)	pH	Conductivity (mV)	TDS (mg L^{-1})
			N	E					
1	*Ie Seu'um*	SH1	5°32.842′	95°32.918′	70	86.02 ± 0.019	6.66 ± 0.000	24.6 ± 0.22	1558 ± 8.37
		SH2	5°32.834′	95°32.924′	72	86.09 ± 0.005	6.66 ± 0.012	24.5 ± 0.28	1766 ± 8.94
		SH3	5°32.821′	95°32.926′	72	83.63 ± 0.075	6.68 ± 0.004	23.0 ± 0.96	1578 ± 5.70
2	*Ie Jue*	JH1	5°30.397′	95°37.683′	264	98.62 ± 0.151	5.93 ± 0.005	76.24 ± 0.74	530.2 ± 5.93
		JH2	5°30.414′	95°37.736′	265	93.62 ± 0.284	4.18 ± 0.107	18.86 ± 0.23	891.8 ± 2.58
		JH3	5°30.403′	95°37.743′	265	93.49 ± 0.172	3.95 ± 0.048	215.78 ± 1.48	997.0 ± 1.73
		JH4	5°30.383′	95°37.743′	269	97.61 ± 0.058	4.92 ± 0.034	149.96 ± 0.98	1125.4 ± 5.55
3	*Ie Brôuk*	IB1	5°31.077′	95°37.034′	210	40.04 ± 0.013	7.24 ± 0.004	14.02 ± 1.01	265.0 ± 1.58
		IB2	5°31.048′	95°36.948′	197	47.49 ± 0.133	7.40 ± 0.058	22.44 ± 0.61	237.60 ± 0.54
4	Van Heutz	VH1	5°28.227′	95°39.491′	723	76.6 ± 0.08	1.57 ± 0.01	9.67 ± 0.10	4.85 ± 0.01
		VH2	5°28.234′	95°39.494′	723	68.5 ± 0.04	1.81 ± 0.01	8.79 ± 0.01	4.39 ± 0.01
		VH3	5°28.237′	95°39.494′	720	46.8 ± 0.11	1.44 ± 0.01	7.28 ± 0.01	3.64 ± 0.01

4.1.2. Hydrothermal Chemical Composition

Tables 5 and 6 show the cation and anion concentration analysis results. This data is further used to estimate the depth temperature using Na-K-Ca and Na-K geothermometry equations, the chemical equilibrium determination of the geothermal water, and the type of geothermal water. The use of ICP to quantify the metal ions in this research showed a significant increase in precision compared to the use of flame ionization in previous research [25–27]. The *Sc* value resulting from repetitive measurements using ICP is much lower than with flame ionization, especially the alkali metal measurements. This the *Sc* value of potassium and sodium resulting from measurement using ICP was in the 0.001–0.008 range, whereas for flame ionization it was in the 0.110–0.260 range.

Table 5. Cation concentration of the geothermal manifestation in Seulawah Agam mountain.

Code	$[K^+] \pm Sc$ (mg L^{-1})	$[Na^+] \pm Sc$ (mg L^{-1})	$[Mg^{2+}] \pm Sc$ (mg L^{-1})	$[Ca^{2+}] \pm Sc$ (mg L^{-1})	$[Li^+] \pm Sc$ (mg L^{-1})	$[B^+] \pm Sc$ (mg L^{-1})	$[SiO_2] \pm Sc$ (mg L^{-1})
SH1	219.26 ± 0.002	1948.8 ± 0.008	10.84 ± 0.125	234.80 ± 0.017	8.03 ± 0.0003	29.10 ± 0.026	15.28 ± 3.69
SH2	218.92 ± 0.001	1951.6 ± 0.007	10.64 ± 0.124	233.51 ± 0.016	7.99 ± 0.0001	29.03 ± 0.028	18.37 ± 1.22
SH3	216.95 ± 0.002	1922.2 ± 0.008	10.13 ± 0.008	234.60 ± 0.018	7.88 ± 0.0002	29.02 ± 0.027	23.95 ± 2.23
JH1	12.10 ± 0.001	11.71 ± 0.007	5.01 ± 0.124	35.56 ± 0.018	nd	0.02 ± 0.026	24.21 ± 2.26
JH2	5.44 ± 0.002	13.54 ± 0.006	5.59 ± 0.123	22.51 ± 0.016	nd	0.07 ± 0.025	19.56 ± 1.49
JH3	7.56 ± 0.002	9.91 ± 0.007	9.22 ± 0.123	50.40 ± 0.018	nd	0.03 ± 0.027	22.04 ± 1.94
JH4	21.87 ± 0.001	48.66 ± 0.008	52.22 ± 0.125	304.56 ± 0.017	nd	0.06 ± 0.026	21.03 ± 1.77
IB1	18.30 ± 0.001	76.88 ± 0.006	6.29 ± 0.124	23.73 ± 0.018	nd	0.232 ± 0.026	19.72 ± 1.53
IB2	18.97 ± 0.002	67.21 ± 0.007	11.58 ± 0.125	27.74 ± 0.017	nd	0.251 ± 0.027	12.82 ± 3.48
VH1	8.74 ± 0.43	34.11 ± 0.72	13.49 ± 0.63	180.86 ± 1.55	0.39 ± 0.01	0.03 ± 0.01	90.05 ± 3.13
VH2	3.47 ± 0.37	5.61 ± 0.54	2.41 ± 0.58	20.18 ± 0.67	0.01 ± 0.01	0.03 ± 0.01	27.27 ± 2.65
VH3	4.01 ± 0.37	4.18 ± 0.53	3.29 ± 0.58	10.69 ± 0.58	0.03 ± 0.02	0.23 ± 0.02	99.87 ± 3.21

Table 6. Anion concentration of geothermal manifestation in Seulawah Agam mountain.

Code	$[Cl^-] \pm Sc$ (mg L^{-1})	$[SO_4^{2-}] \pm Sc$ (mg L^{-1})	$[F^-] \pm Sc$ (mg L^{-1})	$[NO^{3-}] \pm Sc$ (mg L^{-1})	$[HCO^{3-}] \pm Sd$ (mg L^{-1})
SH1	2713.26 ± 0.193	182.46 ± 0.178	nd	nd	104.99 ± 0.55
SH2	2657.77 ± 0.194	160.92 ± 0.177	nd	nd	103.87 ± 0.65
SH3	2671.42 ± 0.193	143.66 ± 0.176	nd	nd	101.09 ± 0.38
JH1	3.34 ± 0.168	11.71 ± 0.007	nd	1.21 ± 0.33	0.54 ± 0.03
JH2	9.74 ± 0.175	13.54 ± 0.006	nd	0.25 ± 0.34	5.45 ± 0.29
JH3	0.80 ± 0.165	9.91 ± 0.007	nd	nd	nd
JH4	1.41 ± 0.166	48.66 ± 0.008	nd	46.75 ± 0.42	nd
IB1	5.31 ± 0.171	76.88 ± 0.006	nd	5.21 ± 0.34	262.81 ± 0.88
IB2	8.66 ± 0.174	67.21 ± 0.007	0.03 ± 0.091	4.68 ± 0.34	255.11 ± 0.62
VH1	12.38 ± 0.12	3127.15 ± 3.06	nd	nd	nd
VH2	0.51 ± 0.10	2641.64 ± 2.82	nd	nd	nd
VH3	0.77 ± 0.10	2597.73 ± 2.79	nd	nd	nd

4.1.3. Chemical Composition of Gases

The analysis results for condensable and non-condensable fumarole gases (Table 7) are calculated in the form of a dry gas percentage (%). The fumarole gas content of the *Ie-Jue* manifestation suggests CO_2 as a dominant gas (93.9%) followed by H_2S (1.02%) and N_2 (3.80%), and minor amount gases (NH_3, Ar, CH_4, and H_2) with ≤ 1% content.

Table 7. Analysis data of fumarole gas from Ie-Jue manifestation.

Source	Location	Coordinates N	E	Elevation (M)	Dry gas mol percentage (%) CO$_2$	H$_2$S	NH$_3$	Ar	N$_2$	CH$_4$	H$_2$
Fumarole	*Ie-Jue*	5°30.037′	95°37.809′	273	93.9	1.02	0.779	0.058	3.80	0.259	0.139

4.2. Hydrochemical Processes

4.2.1. Chemical Composition and Geothermal Water Type

The determination of the dominant chemical components in the geothermal water is presented as a Piper diagram (Figure 2a). Based on the diagram, it is suggested that the *Ie-Seu'um* manifestation at points SH1, SH2 and SH3 has a dominant sodium-potassium-chloride (Na-K-Cl) chemical composition. The *Ie-Jue* manifestation at points JH1, JH2, JH3 and JH4, and the Van Heutz crater manifestation at points VH1, VH2 and VH3 have a dominant calcium-sulphate (Ca-SO$_4$) chemical composition. Meanwhile, the *Ie-Brôuk* manifestation at points IB1 and IB2 has a dominant sodium-calcium-bicarbonate (Na-Ca-HCO$_3$) chemical composition.
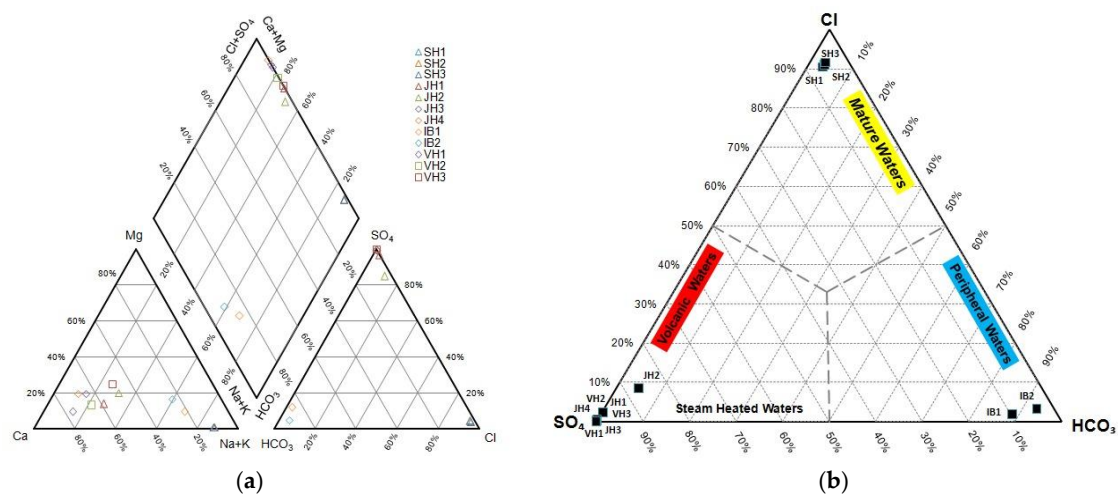
Figure 2. (**a**) Piper diagram for the dominant composition of anion and cation contents; (**b**) Cl-HCO$_3$-SO$_4$ triangle diagram for the geothermal water type in the north zone of Seulawah Agam Mountain.

The type of geothermal water is determined based on the dominant anion content of the water, described by the Cl-HCO$_3$-SO$_4$ triangle diagram (Figure 2b). The diagram indicates that the *Ie-Seu'um* manifestation on average has a chloride type water, *Ie-Brôuk* has on average a bicarbonate type water and *Ie-Jue* and Van-Heutz crater manifestation on average has sulphate type water. The sulphate type water in *Ie-Jue* manifestation suggests a steam-heated water nature. Meanwhile, the sulphate type water along with high acidity of the Van-Heutz crater manifestation is associated with the interaction between magmatic volatility (steam) and groundwater [42].

4.2.2. Na–K–Mg Triangle Diagram

The Na-K-Mg triangle diagram is an indicator used to describe the water equilibrium at high temperature, the process effect of shallow water and the possibility of water equilibria at low temperature [42] Figure 3 indicates that the *Ie-Seu'um* (SH1, SH2, and SH3) area is under partial equilibration conditions, which is a characteristic of mature water. This may be ascribed to the dissolution equilibrium of Na-K and K-Mg minerals in the deep reservoir, hence unaffected by the other mineral dissolution when reaching the surface [34]. Generally, this equilibrium is often found at chloride dominant reservoir types, such as Salton-California's seawater [30].

In contrast with *Ie-Jue*, in the *Ie-Brôuk*, and Van-Heutz crater manifestations, the geothermal water equilibrium is located at an immature waters condition, indicating that the geothermal water is not in equilibrium. This condition also suggests the presence of surface water influence that is mixed at the formation of the hot springs and the interaction between water and rocks in heated conditions [34].
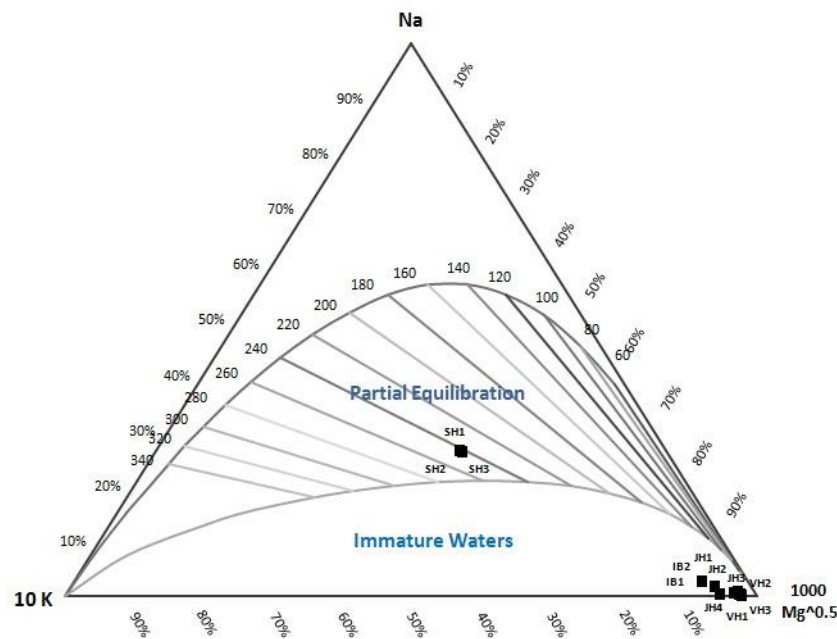
Figure 3. Triangle diagram of Na-K-Mg in Seulawah Agam Mountain Area.

4.3. Estimation of Depth Temperature with Geothermometer

4.3.1. Hydrothermal Geothermometry

Na-K geothermometry is used to estimate a reservoir's temperature based on the Na and K contents in the geothermal fluids. Many studies have developed geothermometers such as Fournier [40], Truesdell [37], Giggenbach [34], Tonani [36], Nieva and Nieva [38], and Arnorsson [38]. This geothermometry technique can be applied well for geothermal fluids with a 180–350 °C reservoir temperature and with low calcium content (CCa$\frac{1}{2}$/Can < 1), as well as for low temperatures (less than 120 °C [30]).

Table 8 is the estimation of the reservoir depth temperature of a geothermal manifestation employing some Na-K geothermometers. Based on the Giggenbach Na-K geothermometer [34], the reservoir's temperatures of the *Ie-Seu'um* and *Ie-Br*ôuk manifestations are at 241.9–242.2 °C (with the an average temperature of 241.9 ± 0.3 °C) and 312.5–331.4 °C (with an average temperature of 321.95 ± 13.4 °C), respectively, whereas the reservoir temperature of *Ie-Jue* and the Van-Heutz crater manifestations are on average >350 °C. For the stated conditions, according to Nicholson [30], it is suggested to use the Fournier Na-K geothermometer [35]. Based on the Fournier Na-K geothermometer [35], the reservoir temperatures of *Ie-Jue* and the Van-Heutz crater manifestations are 374.5–555.4 °C (with the average temperature of 472.4 ± 91.4 °C) and 331.2–511.3 °C (with the average temperature of 439.3 ± 95.3 °C), respectively.

Table 8. Estimation of reservoir's temperature of geothermal areas in north zone Seulawah Agam mountain.

Sampling Point	Na-K-Ca Fournier & Truesdell (1973) (°C)	Na/K Fournier (1979) (°C)	Na/K Truesdell (1976) (°C)	Na/K Giggenbach (1988) (°C)	Na/K Tonani (1980) (°C)	Na/K Nieva & Nieva (1987) (°C)	Na/K Arnorsson (1983) (°C)
SH1	210.7	227.3	200.6	241.9	237.6	213.9	207.3
SH2	210.6	227.0	200.6	241.6	237.2	213.6	207.0
SH3	210.6	227.6	200.9	242.2	238.0	214.1	207.7
JH1	69.2	555.4	741.7	527.6	879.9	536.0	680.1
JH2	55.9	374.5	409.5	374.6	477.7	358.1	398.5
JH3	47.3	487.2	604.5	471.1	710.6	468.9	567.0
JH4	58.3	391.8	437.1	389.6	510.1	375.1	423.0
BH1	115.1	304.6	304.7	312.5	356.1	289.6	304.1
BH2	110.7	325.7	335.1	331.4	391.1	310.2	331.8
VH1	41.3	331.2	343.3	336.3	400.6	315.7	339.2
VH2	39.2	475.4	582.4	461.2	683.8	457.3	548.3
VH3	49.0	511.3	651.1	491.3	767.6	492.6	605.9

4.3.2. Gas Geothermometry

Gas Geothermometer

Gas geothermometry has been developed to estimate a reservoir's temperature based on the CO_2, H_2S, NH_3, CH_4, N_2, H_2, and Ar contents in fumarole gas. Some gas geothermometers have been developed by D'Amore and Panichi [44]; Giggenbach and Goguel [34]; Giggenbach [42]. The *Ie-Jue* manifestation is a fumarole type manifestation from the north zone of Seulawah Agam mountain. Based on the gas geothermometer calculations, the temperature of the fumarole reservoir of the *Ie-Jue* manifestation is at 201.6–312.7 °C (with an average temperature of 258.85 °C) (Table 9).

Table 9. Estimation of depth temperature using gas geothermometer.

Location	Gas Geothermometer (T = °C)			
	$CO_2/H_2S/CH_4/H_2$	H_2/Ar	CH_4/CO_2	CO_2/H_2
Ie Jue	256.2	201.6	316.7	260.9

FT-CO_2 Cross-Plot and CH_4-CO_2-H_2S Triangle Diagram

Reservoir temperatures can be estimated with a FT-CO_2 cross-plot and a CH_4-CO_2-H_2S triangle diagram [46]. The reservoir temperature estimation with FT-CO_2 cross-plot is conducted based on the dominant CO_2 gas, while for the CH_4-CO_2-H_2S triangle diagram, the estimation is done based on the degassing process of a geothermal fluid when reaching the surface [47]. Based on the FT-CO_2 cross-plot (Figure 4a), the *Ie-Jue* fumarole manifestation points (JH) are located on an imaginary line with a temperature range between 275–300 °C. This also indicates that the reservoir is liquid-dominated. Based on the CH_4-CO_2-H_2S triangle diagram, the *Ie-Jue* fumarole manifestation has a reservoir temperature of 300–325 °C. Based on the estimation of both the FT-CO_2 cross-plot and CH_4-CO_2-H_2S triangle diagram, it can be concluded that the reservoir temperature of the manifestation is around 275–325 °C.
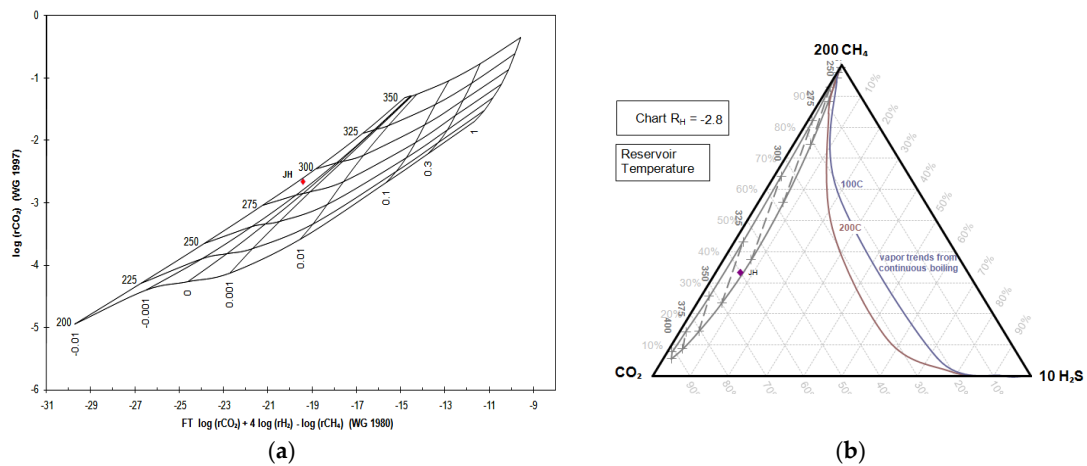
Figure 4. (**a**) FT-CO$_2$ cross-plot diagram and (**b**) CH$_4$-CO$_2$-H$_2$S triangle diagram.

N$_2$-He-Ar Triangle Diagram

The N$_2$-He-Ar triangle diagram is a mixing diagram model used to portray the relative contribution of the gas sources, whether the gas is magmatic, meteoric, or Earth's crust sourced. The content proportions of N$_2$, He and Ar have been combined by Giggenbach [34] for the identification of dominant gas sources in a fumarole gas manifestation [30]. The triangle diagram of N$_2$-He-Ar (Figure 5) shows that the point position of the *Ie-Jue* fumarole gas manifestation (JH) is adjacent to water vapor content at a N$_2$/Ar ratio near 84. This indicates that the source of *Ie-Jue* fumarole gas is of meteoric origin.
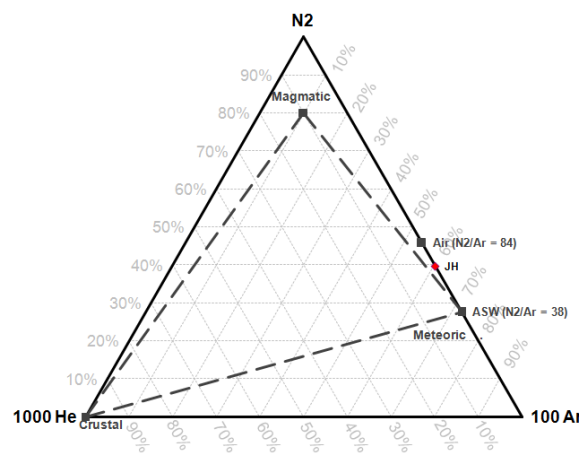
Figure 5. N$_2$-He-Ar triangle diagram.

4.4. Isotope Analysis

The results of the determination of oxygen (δ^{18}O) and deuterium (δ^2H) isotopes for the geothermal area in the north zone of Seulawah Agam can be seen in Table 10. The values of both isotopes are then correlated against the V-SMOW international standard lines to describe the origins of the geothermal water, whether it is meteoric, magmatic or a mixture of both.

Based on the isotope ratio in the stable isotope plot (Figure 6), the *Ie-Seu'um, Ie-Jue, Ie-Brôuk,* and *Ie-Jue* (only JH4), manifestations are originated from meteoric water. This is indicated by the manifestation points, which are adjacent to the local meteoric water line (LMWL). Only some points present on the mixing line water, such as the JH1, JH2 and JH3 sampling points of the *Ie-Jue* manifestation display positive values for the isotope δ^{18}O, while the Van-Heutz crater manifestation (VH1, VH2, and VH3) is of magmatic water origin. This is indicated by the positive value of the isotope δ^{18}O. The shift

of isotope $\delta^{18}O$ value to a positive direction is due to the heavier isotope exchange reaction, leading to a contribution of magmatic water in a hot spring.

Table 10. Value of δ^18O and δ^2H stable isotopes.

Sampling Point	$\delta^{18}O$ (‰)	δ^2H (‰)
SH1	-6.85 ± 0.05	-54.7 ± 2.3
SH2	-7.75 ± 0.23	-51.7 ± 0.8
SH3	-5.95 ± 0.32	-49.9 ± 0.3
JH1	-1.29 ± 0.55	-37.8 ± 2.9
JH2	-0.23 ± 0.24	-31.0 ± 0.7
JH3	-0.19 ± 0.37	-32.4 ± 0.8
JH4	-5.34 ± 0.18	-46.0 ± 0.4
IB1	-9.09 ± 0.27	-53.7 ± 2.1
IB2	-9.66 ± 0.57	-53.4 ± 0.5
VH1	4.42 ± 0.28	-12.4 ± 2.1
VH2	6.44 ± 0.16	-7.7 ± 4.8
VH3	4.50 ± 0.14	-7.1 ± 0.9
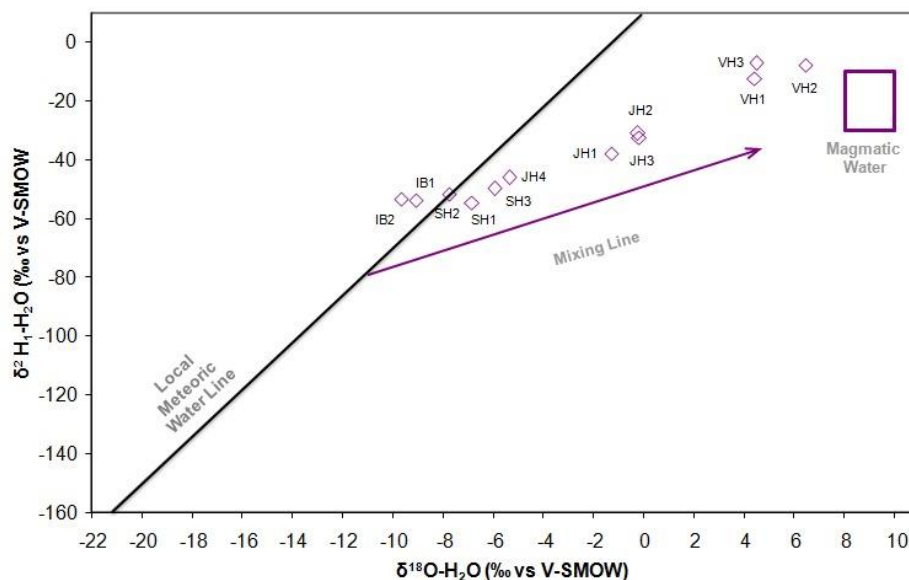
Figure 6. $\delta^{18}O$ dan δ^2H stable isotope plot.

This phenomenon also occurs in Ijen crater (Jawa Timur) with a prediction that some magmatic water is discharged through fumaroles up until 70% from the geothermal water composition [10,43].

5. Conclusions

This study concerns the four geothermal system manifestations (*Ie-Seu'um*, *Ie-Brouk*, *Ie-Jue*, and Van-Heutz crater) of the Selawah Agam volcano, located in northwestern Sumatra, Indonesia. The analysis of the Cl-HCO$_3$-SO$_4$ triangle diagram and Piper diagram suggests that the water type and dominant chemical composition of the fluids of each manifestation are as follows: (1) chloride and Na-K-Cl for *Ie-Seu'um*, (2) bicarbonate and Na-Ca-HCO$_3$ for *Ie-Brouk* and (3) sulphate and Ca-SO$_4$ for *Ie-Jue* and the Van-Heutz crater.

The analysis of the Na-K-Mg triangle diagram suggests that the fluid equilibrium of *Ie-Brôuk*, *Ie-Jue*, and Van-Heutz crater manifestations presents an immature water state. Only the fluid from the *Ie-Seu'um* manifestation is in a mature water state.

The analysis of the isotope ratio in the stable isotope plot showed that the water of *Ie-Seu'um*, *Ie-Jue*, *Ie-Brôuk,* and *Ie-Jue* are originated from meteoric water. While the Van-Heutz crater manifestation is originated from magmatic water.

The Giggenbach Na-K hydrothermal geothermometer [34] indicates that the *Ie-Seu'um* and *Ie-Brôuk* manifestations have average reservoir temperatures of 241.9 ± 0.3 °C a d 321.95 ± 13.4 °C, respectively, wheras the Fournier Na-K hydrothermal geothermometer [35] indicates that the *Ie-Jue* and Van-Heutz crater manifestations have average reservoir temperatures of 472.4 ± 91.4 °C and 439.3 ± 95.3 °C, respectively.

Gas geothermometry indicates that the *Ie-Jue* fumarole manifestation has a reservoir temperature of 201.6–312.7 °C. The analysis of the FT-CO_2 Cross-Plot and CH_4-CO_2-H_2S triangle diagram on the fumarole manifestation shows the reservoir temperature to be 275–325 °C. The analysis of the N_2-He-Ar triangle diagram suggests that the *Ie-Jue* fumarole gas is of meteoric water origin.

Based on the reservoir temperatures, that can be estimated well using gas geothermometry and fluid geothermometry, the geothermal manifestations of the north zone of Seulawah Agam mountain are considered to constitute a high-temperature geothermal system (high enthalpy) in accordance with Hochstein, which is indicated by the average measured temperature > 225 °C. This condition suggests that the geothermal area is suitable for power plant development. In accordance with Kasbani [48] regarding the estimation of the energy potential for different geothermal types in Indonesia, the estimated capacity of the power plant production based on this temperature is above 100 MW and is estimated to have a reservoir with a system type dominated by steam and water or a mixture of both.

Author Contributions: Conceptualization, R.I. and T.M.I.M.; Data curation, M.Y., M.A., S.S. (Subhan Subhan), A.L., G.M.I. and M.M. (Marwan Marwan); Formal analysis, R.I., M.Y., M.A., S.S. (Subhan Subhan) and A.L.; Funding acquisition, R.I. and T.M.I.M.; Investigation, R.I.; Methodology, R.I. and S.S. (Saiful Saiful); Resources, M.M. (Marwan Marwan); Software, R.S. and G.M.I.; Supervision, R.I.; Validation, M.M. (Muslem Muslem); Visualization, R.S.; Writing—original draft, M.Y.; Writing—review & editing, R.I., M.M. (Muslem Muslem) and T.M.I.M.

Conflicts of Interest: The authors declare no conflict of interest.

References

1. Ong, H.C.; Masjuki, H.H.; Mahlia, T.M.I.; Silitonga, A.S.; Chong, W.T.; Yusaf, T. Engine performance and emissions using Jatropha curcas, Ceiba pentandra and Calophyllum inophyllum biodiesel in a CI diesel engine. *Energy* **2014**, *69*, 427–445. [CrossRef]
2. Silitonga, A.S.; Masjuki, H.H.; Mahlia, T.M.I.; Ong, H.C.; Chong, W.T. Experimental study on performance and exhaust emissions of a diesel engine fuelled with Ceiba pentandra biodiesel blends. *Energy Conversion and Management* **2013**, *76*, 828–836. [CrossRef]
3. Ismail, M.S.; Moghavvemi, M.; Mahlia, T.M.I. Techno-economic analysis of an optimized photovoltaic and diesel generator hybrid power system for remote houses in a tropical climate. *Energy Convers. Manag.* **2013**, *69*, 163–173. [CrossRef]
4. Ismail, M.S.; Moghavvemi, M.; Mahlia, T.M.I. Characterization of PV panel and global optimization of its model parameters using genetic algorithm. *Energy Convers. Manag.* **2013**, *73*, 10–25. [CrossRef]
5. Amin, M.; Putra, N.; Kosasih, E.A.; Prawiro, E.; Luanto, R.A.; Mahlia, T.M.I. Thermal properties of beeswax/graphene phase change material as energy storage for building applications. *Appl. Eng.* **2017**, *112*, 273–280. [CrossRef]

6.   Mehrali, M.; Latibari, S.T.; Mehrali, M.; Mahlia, T.M.I.; Metselaar, H.S.C.; Naghavi, M.S.; Sadeghinezhad, E.; Akhiani, A.R. Preparation and characterization of palmitic acid/graphene nanoplatelets composite with remarkable thermal conductivity as a novel shape-stabilized phase change material. *Appl. Eng.* **2013**, *61*, 633–640. [CrossRef]

7.   Silitonga, A.S.; Mahlia, T.M.I.; Kusumo, F.; Dharma, S.; Sebayang, A.H.; Sembiring, R.W.; Shamsuddin, A.H. Intensification of Reutealis trisperma biodiesel production using infrared radiation: Simulation, optimisation and validation. *Renew. Energy* **2019**, *133*, 520–527. [CrossRef]

8.   Silitonga, A.; Mahlia, T.M.; Ong, H.C.; Riayatsyah, T.M.; Kusumo, F.; Ibrahim, H.; Dharma, S.; Gumilang, D. A comparative study of biodiesel production methods for Reutealis trisperma biodiesel. *Energy Sources Part A Recover. Util. Environ. Eff.* **2017**, *39*, 2006–2014. [CrossRef]

9.   Silitonga, A.S.; Masjuki, H.H.; Ong, H.C.; Sebayang, A.H.; Dharma, S.; Kusumo, F.; Siswantoro, J.; Milano, J.; Daud, K.; Mahlia, T.M.I.; et al. Evaluation of the engine performance and exhaust emissions of biodiesel-bioethanol-diesel blends using kernel-based extreme learning machine. *Energy* **2018**, *159*, 1075–1087. [CrossRef]

10.   Hochstein, M.P.; Sudarman, S. History of geothermal exploration in Indonesia from 1970 to 2000. *Geothermics* **2008**, *37*, 220–266. [CrossRef]

11.   Maryanto, S.; Dewi, C.N.; Syahra, V.; Rachmansyah, A.; Foster, J.; Nadhir, A.; Santoso, D.R. Magnetotelluric-geochemistry investigations of blawan geothermal field, East Java, Indonesia. *Geosciences* **2017**, *7*, 41. [CrossRef]

12.   Bertani, R. Geothermal power generation in the world 2010–2014 update report. *Geothermics* **2016**, *60*, 31–43. [CrossRef]

13.   Nasruddin; Alhamid, M.I.; Daud, Y.; Surachman, A.; Sugiyono, A.; Aditya, H.B.; Mahlia, T.M.I. Potential of geothermal energy for electricity generation in Indonesia: A review. *Renew. Sustain. Energy Rev.* **2016**, *53*, 733–740. [CrossRef]

14.   Guo, Q.; Pang, Z.; Wang, Y.; Tian, J. Fluid geochemistry and geothermometry applications of the Kangding high-temperature geothermal system in eastern Himalayas. *Appl. Geochem.* **2017**, *81*, 63–75. [CrossRef]

15.   Ármannsson, H. The fluid geochemistry of Icelandic high temperature geothermal areas. *Appl. Geochem.* **2016**, *66*, 14–64. [CrossRef]

16.   Cinti, D.; Procesi, M.; Tassi, F.; Montegrossi, G.; Sciarra, A.; Vaselli, O.; Quattrocchi, F. Fluid geochemistry and geothermometry in the western sector of the Sabatini Volcanic District and the Tolfa Mountains (Central Italy). *Chem. Geol.* **2011**, *284*, 160–181. [CrossRef]

17.   Tan, H.; Zhang, W.; Chen, J.; Jiang, S.; Kong, N. Isotope and geochemical study for geothermal assessment of the Xining basin of the northeastern Tibetan Plateau. *Geothermics* **2012**, *42*, 47–55. [CrossRef]

18.   Wang, A.; Padula, A.; Sirota, M.; Woodruff, T.J. Environmental influences on reproductive health: The importance of chemical exposures. *Fertil. Steril.* **2016**, *106*, 905–929. [CrossRef]

19.   Rafighdoust, Y.; Eckstein, Y.; Harami, R.M.; Gharaie, M.H.M.; Griffith, E.M.; Mahboubi, A. Isotopic analysis, hydrogeochemistry and geothermometry of Tang-Bijar oilfield springs, Zagros region, Iran. *Geothermics* **2015**, *55*, 24–30. [CrossRef]

20.   Joseph, E.P.; Fournier, N.; Lindsay, J.M.; Robertson, R.; Beckles, D.M. Chemical and isotopic characteristics of geothermal fluids from Sulphur Springs, Saint Lucia. *J. Volcanol. Geotherm. Res.* **2013**, *254*, 23–36. [CrossRef]

21.   Capaccioni, B.; Franco, T.; Alberto, R.; Orlando, V.; Marco, M.; Salvatore, I. Geochemistry of thermal fluids in NW Honduras: New perspectives for exploitation of geothermal areas in the southern Sula graben. *J. Volcanol. Geotherm. Res.* **2014**, *280*, 40–52. [CrossRef]

22.   Pasvanoğlu, S.; Chandrasekharam, D. Hydrogeochemical and isotopic study of thermal and mineralized waters from the Nevşehir (Kozakli) area, Central Turkey. *J. Volcanol. Geotherm. Res.* **2011**, *202*, 241–250. [CrossRef]

23.   Marwan; Yanis, M.; Idroes, R.; Ismail, N. 2D inversion and static shift of MT and TEM data for imaging the geothermal resources of Seulawah Agam Volcano, Indonesia. *Int. J. Geomate* **2019**, *17*, 173–180. [CrossRef]

24.   Marwan; Syukri, M.; Idroes, R.; Ismail, N. Deep and shallow structures of geothermal Seulawah Agam based on electromagnetic and magnetic data. *Int. J. Geomate* **2019**, *16*, 141–147. [CrossRef]

25. Idroes, R.; Yusuf, M.; Alatas, M.; Lala, A.; Suhendra, R.; Idroes, G.M. Geochemistry of hot springs in the Ie Seu'um hydrothermal areas at Aceh Besar district, Indonesia. In Proceedings of the International Conference on Chemical Engineering Sciences and Applications, Banda Aceh, Indonesia, 21 September 2017; IOP Conference Series: Materials Science and Engineering. IOP Publishing: Bristol, UK, 2018; Volume 334.

26. Idroes, R.; Yusuf, M.; Alatas, M.; Subhan; Lala, A.; Muhammad; Suhendra, R.; Idroes, G.M.; Marwan. Geochemistry of sulphate spring in the Ie Jue geothermal areas at Aceh Besar district, Indonesia. In Proceedings of the Annual International Conference, Banda Aceh, Indonesia, 12 September 2018; IOP Conference Series: Materials Science and Engineering. IOP Publishing: Bristol, UK, 2019; Volume 523, p. 012012.

27. Idroes, R.; Yusuf, M.; Alatas, M.; Subhan; Lala, A.; Muslem; Suhendra, R.; Idroes, G.M.; Suhendrayatna; Marwan; et al. Geochemistry of warm springs in the Ie Brôuk hydrothermal areas at Aceh Besar district. In Proceedings of the Annual International Conference, Banda Aceh, Indonesia, 12 September 2018; IOP Conference Series: Materials Science and Engineering. IOP Publishing: Bristol, UK, 2019; Volume 523, p. 012010.

28. Lahna, K.; Idroes, R.; Idris, N.; Abdulmadjid, S.N.; Kurniawan, K.H.; Tjia, M.O.; Pardede, M.; Kagawa, K. Formation and emission characteristics of CN molecules in laser induced low pressure He plasma and its applications to N analysis in coal and fossilization study. *Appl. Opt.* **2016**, *55*, 1731. [CrossRef]

29. Marpaung, A.M.; Ramli, M.; Idroes, R.; Suyanto, H.; Lahna, K.; Abdulmadjid, S.N.; Idris, N.; Pardede, M.; Hedwig, R.; Lie, Z.S. A comparative study of emission efficiencies in low-pressure argon plasmas induced by picosecond and nanosecond Nd:YAG lasers. *Jpn. J. Appl. Phys.* **2016**, *55*, 116101. [CrossRef]

30. Nicholson, K. *Geothermal Fluids*; Springer: Berlin/Heidelberg, Germany, 1993; ISBN 978-3-642-77846-9.

31. APHA. *Standard Methods for the Examination of Water and Wastewater*, 21st ed.; American Public Health Association/American Water Works Association/Water Environment Federation: Washington, DC, USA, 2005.

32. Craig, H. The isotopic geochemistry of water and and carbon in geothermal areas. In *Nuclear Geology in Geothermal Areas, Spoleto*; Tiongiorgi, E., Ed.; Consiglio Nazional delle Ricerche, Laboratorio di Geologia Nucleare, Pias: Rome, Italy, 1963; pp. 17–53.

33. Giggenbach, W.F.; Goguel, R.L. *Collection and Analysis of Geothermal and Volcanic Water and Gas Discharges*, 4th ed.; Report CD2401; Chemistry Division, DSIR: Petone, New Zealand, 1989.

34. Giggenbach, W.F. Geothermal solute equilibria. Derivation of Na-K-Mg-Ca geoindicators. *Geochim. Cosmochim. Acta* **1988**, *52*, 2749–2765. [CrossRef]

35. Fournier, R.O. A revised equation for the Na/K Geothermometer. *Geotherm. Resour. Council Trans.* **1979**, *3*, 221–224.

36. Tonani, F.B. Some Remarks on the Application of Geochemical Techniques in geothermal exploration. In *Advances in European Geothermal Research*; Springer Netherlands: Dordrecht, The Netherlands, 1980; pp. 428–443.

37. Truesdell, H. Geochemical Techniques in Exploration: Summary of Section III. In Proceedings of the Second UN Symposium on the Development and Use of Geothermal Resources, San Francisco, CA, USA, 20 May 1976; pp. 53–79.

38. Nieva, D.; Nieva, R. Developments in geothermal energy in Mexico—part twelve. A cationic geothermometer for prospecting of geothermal resources. *Heat Recover. Syst. CHP* **1987**, *7*, 243–258. [CrossRef]

39. Arnorsson, S. Chemical equilibria in icelandic geothermal systems—Implications for chemical geothermometry investigations. *Geothermics* **1983**, *12*, 119–128. [CrossRef]

40. Fournier, R.O.; Truesdell, H. An empirical Na-K-Ca geothermometer for natural waters. *Geochimica et Cosmochimica Acta* **1973**, *37*, 1255–1275. [CrossRef]

41. Piper, A.M. A graphic procedure in the geochemical interpretation of water-analyses. *Trans. Am. Geophys. Union* **1944**, *25*, 914. [CrossRef]

42. Giggenbach, W.F. Chemical techniques in geothermal exploration. In *Applications of Geochemistry in Geothermal Reservoir Development*; D'Amore, F., Ed.; UNITAR/UNDP: Rome, Italy, 1991; pp. 119–144.

43. Giggenbach, W.F. Isotopic shifts in waters from geothermal and volcanic systems along convergent plate boundaries and their origin. *EPSL* **1992**, *113*, 495–510. [CrossRef]

44. D' Amore, F.; Panichi, C. Evaluation of deep temperatures of hydrothermal systems by a new gas-geothermometer. *Geochim. Cosmochim. Acta* **1980**, *44*, 549–556. [CrossRef]

45. Douglas, A.S.; Donald, M.W.; Holler, F.; Crouch, S. *Fundamentals of Analytical Chemistry. Saunders Golden Sunburst Series*; Thomson-Brooks/Cole: Hampshire, UK, 2004.
46. Giggenbach, W.F.; Glover, R.B. Tectonic regime and major processes governing the chemistry of water and gas discharges from the rotorua geothermal field, New Zealand. *Geothermics* **1992**, *21*, 121–140. [CrossRef]
47. Powell, T.; Cumming, W. Spreadsheets for Geothermal Water and Gas Geochemistry. In Proceedings of the Thirty-Fifth Workshop on Geothermal Reservoir Engineering Stanford University, Stanford, CA, USA, 1–3 February 2010; pp. 408–417.
48. Kasbani. Tipe sistem panas bumi di Indonesia dan estimasi potensi energinya. *Buletin Sumber Daya Energi* **2009**, *4*, 3.